Sensors and Materials, Vol. 37, No. 7 (2025) 3181–3189
MYU Tokyo

S & M 4111

Effect of Binary Solvent System of Methyl Acetate and Chlorobenzene on Crystallization of Perovskite

Cheng-En Chang,[1] Jenn-Kai Tsai,[1*] Zheng-Wei Li,[1]
Tian-Chiuan Wu,[1] Teen-Hang Meen,[1] and Chi-Ting Ho[2]

[1]Department of Electronic Engineering, National Formosa University, Yunlin 632, Taiwan
[2]Department of Mechanical Design Engineering, National Formosa University, Yunlin 632, Taiwan

(Received January 27, 2025; accepted July 7, 2025)

Keywords: perovskite solar cells, MAPbI3, methyl acetate, chlorobenzene, antisolvent

Perovskite solar cells (PSCs) have attracted widespread attention owing to their high photovoltaic conversion efficiency and low manufacturing costs. The crystallinity of the PSC film significantly affects the PSC's photoelectric conversion efficiency. In this study, the crystallinity of the perovskite film was investigated by changing the mixing ratio of two antisolvents [methyl acetate (MA) and chlorobenzene (CB)] to optimize the preparation of the perovskite film. The use of MA as an antisolvent resulted in the formation of perovskite crystals with an average size of 182 nm, with the largest size reaching 498 nm. However, the pores had a detrimental impact on the photovoltaic conversion efficiency. The addition of CB at varying proportions increased the average size of perovskite crystals to 348 nm. With 40 vol% CB, the largest crystals showed a size of 772 nm. Furthermore, the number of pores was significantly reduced, and surface roughness was diminished to 17.6 nm, resulting in a photovoltaic conversion efficiency of 1.54%. However, 50 vol% CB stratified the perovskite layer, which decreased the grain size, surface roughness, and photovoltaic conversion efficiency.

1. Introduction

The continuous growth of global energy demand and the increasingly serious environmental problems have necessitated the search for efficient and environmentally friendly renewable energy. In solar energy production, silicon-based solar cells are mainly used owing to their longevity and extensive range of applications. However, the performance of dye-sensitized solar cells (DSSCs) and perovskite solar cells (PSCs) is better than that of silicon-based solar cells. DSSCs and PSCs have attracted considerable interest owing to their low preparation cost, equipment requirements, and easy fabrication on flexible substrates.[1–3] Because PSCs have a particularly high photoelectric conversion efficiency, they have been studied extensively in photovoltaic technology.[4,5]

The dense titianium dioxide (TiO_2) layer used in this study can circumvent the serious recombination phenomenon of electrons and holes. The mesoporous TiO_2 nanoparticle layer has

*Corresponding author: e-mail: tsaijk@nfu.edu.tw
https://doi.org/10.18494/SAM5579

ISSN 0914-4935
https://myukk.org/

a large surface area, which promotes the adsorption of perovskite materials, and provides a good growth space for perovskite films. After annealing, the contact between TiO_2 nanoparticles is enhanced, promoting nanoparticle fusion and reducing resistance at the contact interface between the nanoparticles.[1] This facilitates electron flow from the perovskite layer to the dense TiO_2 layer. These optimization measures improve the photoelectric conversion efficiency of PSCs and enhance their stability and reliability.[6–8]

Antisolvent treatment is important in the enhancement of PSC performance. The choice of the antisolvent and the treatment method considerably impact the quality and performance of the device. Accordingly, appropriate antisolvents and treatment conditions are essential for the enhancement of efficiency.[9]

Methyl acetate (MA) exhibits a high vapor pressure (23.07 kPa) and favorable water solubility compared with other antisolvents. The high vapor pressure and low boiling point facilitate the evaporation of excess dimethylformamide (DMF) and control the perovskite crystallization Furthermore, the high solubility of the antisolvent in water mitigates the impact of moisture in the spin-coating process.[10,11] Compared with antisolvents with high vapor pressure and low boiling point, such as MA, ethyl acetate, butyl acetate, and propyl acetate, CB as a single antisolvent can produce larger perovskite crystals and higher photoelectric conversion efficiency.[12–14]

In this study, we used a mixture of MA and CB as antisolvents to enhance the performance of PSCs. MA has high volatility (3.7, relative to diethyl ether = 1) and high vapor pressure (23.07 kPa), which are sufficiently high to rapidly remove excess solvents from the precursor solution and promote uniform and rapid crystallization. However, owing to its high volatility, films formed using MA may have pinholes and may be nonuniform. On the other hand, CB has low volatility (0.26) and low vapor pressure (1.47 kPa), which assists in the formation of dense and defect-free films.[15,16] By leveraging the high volatility of MA, rapid solvent removal and the uniformity and crystallization quality of the film were ensured owing to the low volatility of CB. The combined use of these two antisolvents resulted in higher efficiency and better film quality than films prepared using only MA or CB as the antisolvent.

Compared with MA or CB alone, the advantages of both antisolvents can be combined by mixing MA with CB. The high volatility of MA ensures the rapid removal of excess solvent, whereas the low volatility of CB helps optimize film uniformity and crystal quality. Eze *et al.* achieved the lowest surface roughness of 13.53 nm and the best photovoltaic conversion efficiency (PCE) of 18.55% by using MA mixed with chloroform at different proportions.[17]

2. Materials and Methods

2.1 Reagents

The following reagents were used in the experiment: fluorine-doped tin oxide (FTO) substrates, indium tin oxide (ITO), Spiro-OMeTAD (99.9%), acetone (99.5%), methyl alcohol (99%), and ethanol (99%) (UNI-ONWARD, Taiwan); titanium diisopropoxide bis(acetylacetonate) (75 wt%) (Sigma-Aldrich, India); zinc powder (97%) and dodecanoic acid (98%) (Alfa Aesar,

Great Britain); dydrochloric acid (37%) (Honeywell Fluka, Australia); 1-butanol, high performance liquid chromatography (HPLC) grade (99%) and alpha-terpineol (96%) (Alfa Aesar, USA); ethyl cellulose (48%) and 4-tert-butylpyridine (tBp, 98%) (Sigma-Aldrich, USA); titanium dioxide (TiO_2 P25, anatase 80% and rutile 20%) and lithium bis(trifluoromethanesulfonyl) imide (LiTFSI, 99%) (Uniregion Bio-Tech, Taiwan); methylammonium iodide (MAI, 99.9%) (STAREK Scientific, Taiwan); lead (II) iodide (PbI_2, 99%) (Sigma-Aldrich, UK); and DMF (99.8%), dimethyl sulfoxide (DMSO, 99.9%), CB (99.5%), and MA (99.5%) (Avantor Performance Materials, USA).

2.2 Cleaning of FTO substrate

FTO substrates were cleaned using an ultrasonic cleaner for 5 min. Acetone was used to eliminate organic impurities and oils from the FTO surface. Subsequently, methanol was used to remove any residual acetone, and deionized water was employed to remove organic solvents. After ultrasonic cleaning, the FTO substrate was dried using a nitrogen gun. Finally, a UV-ozone cleaner was used for 10 min to break down the molecular bonds of any remaining organic substances.

2.3 Fabrication of PSC

The initial layer of the PCS was a compact layer of TiO_2. Before spin coating the dense TiO_2 layer, a 10 mm heat-resistant tape of 10 × 30 mm size was attached above the FTO substrate to demarcate the working area. 0.15 and 0.3 M acetylacetonate and 1-butanol solutions were prepared. 250 μl of the 0.15 M solution was dropped on the working area and spin-coated at 3,000 rpm for 30 s. Once the procedure was complete, the FTO glass was transferred to a heating platform maintained at 120 ℃ for 5 min. Next, 250 μl of the 0.3 M solution was dropped on the working area and spin-coated at 3,000 rpm for 30 s. The FTO glass was then heated on a heating platform at 120 ℃ for 5 min. The above steps were repeated to spin-coat a 0.3 M solution layer. The heat-resistant tape was removed from the FTO substrate, which was then annealed at 550 ℃ for 30 min in a high-temperature furnace.

The second layer was a mesoporous TiO_2 layer. The mesoporous layer solution was prepared by mixing TiO_2 nanoparticles (P25), dodecanoic acid, ethyl cellulose, alpha-terpineol, and ethanol at a specific ratio. 250 μl of the TiO_2 mesoporous layer solution was dropped on the working area and spin-coated at 3,000 rpm for 30 s. Following the spin-coating process, the FTO substrate was heated on a heating platform at 120 ℃ for 5 min. This procedure was repeated, and subsequently, the FTO substrate was annealed at 550 ℃ for 1 h in a high-temperature furnace.

The third layer was the perovskite layer. A one-step method was employed to prepare the perovskite layer. A solution comprising 1 M MAI and 1 M PbI_2 was prepared with a mixed solutions of DMF and DMSO at a volume ratio of 4:1. Given the sensitivity of the perovskite layer to environmental factors, the perovskite layer was prepared in a nitrogen glove box at a relative humidity of 15%. The perovskite layer was stirred at 70 ℃ for 3 h. Subsequently, for

two-stage spin-coating, 250 µl of the perovskite layer solution was dispensed onto the working area and spun at 1,000 rpm for 10 s and at 3,000 rpm for 30 s. Then, the antisolvents were introduced at 10 s. In this study, we varied the ratio of MA to CB from 0 to 50 vol% to prepare the antisolvents, as shown in Table 1. The mixture of MA and CB was the optimal solution as it maintained the advantages of both compounds. The high volatility of MA ensured the rapid removal of excess solvent, whereas the low volatility of CB helped optimize film uniformity and crystallization quality.

The fourth layer was the hole transport layer. A LiTFSI solution was prepared by mixing and stirring 0.52 g of LiTFSI with 1 ml of acetonitrile. Then, 1 ml of CB was added to 0.0723 g of Spiro-OMeTAD. 28.8 µl of tBp and 17.5 µl of LiTFSI solution were stirred until the solution turned purple. The hole transport layer solution was spin-coated onto the substrate at 4,000 rpm for 15 s. Finally, the PSC was fabricated by sputtering 60 nm of Au onto the hole transport material and encapsulating it with ITO glass.

2.4 Characterization

The morphology of the perovskite film was examined by field emission-scanning electron microscopy (FE-SEM, JSM-7610FPlus, JEOL, Tokyo, Japan) and atomic force microscopy (AFM, Bruker, Dimension ICON XR, Billerica, MA, USA). The perovskite crystal size was analyzed in FE-SEM images using Image J (National Institutes of Health, Bethesda, USA). A UV-visible spectrometer (U2900A, Hitachi, Tokyo, Japan) was used to measure the light absorption of the PSC. The crystalline phase of perovskite was analyzed by X-ray diffraction metrology (XRD) (D8, BRUKER, Billerica, MA, USA). The power conversion efficiency of the PSC was determined using a solar simulator (XES 40S1, San Ei Brand, Osaka, Japan) under AM 1.5 (100 mW/cm^2).

3. Results and Discussion

Figure 1 shows the top view of the perovskite layer fabricated using the mixture of MA and CB. Images (a) to (f) illustrate the impact of the CB concentration varied from 0 to 50% on the perovskite film. As the parcentage of CB increased, the size of the perovskite crystals gradually increased.

The morphology of the perovskite film was examined by AFM. Figures 2(a) to 2(f) show the AFM images of the perovskite layer. The smoothness of the perovskite layer surface was improved as the percentage of CB was increased from 20 to 40%.

Figure 3 shows the impacts of CB volume percentage concentration (vol%) on perovskite grain size and surface roughness (Rq). The average and maximum grain sizes gradually

Table 1
Composition of antisolvents used in this study.

Sample	0	10	20	30	40	50
MA (vol%)	100	90	80	70	60	50
CB (vol%)	0	10	20	30	40	50

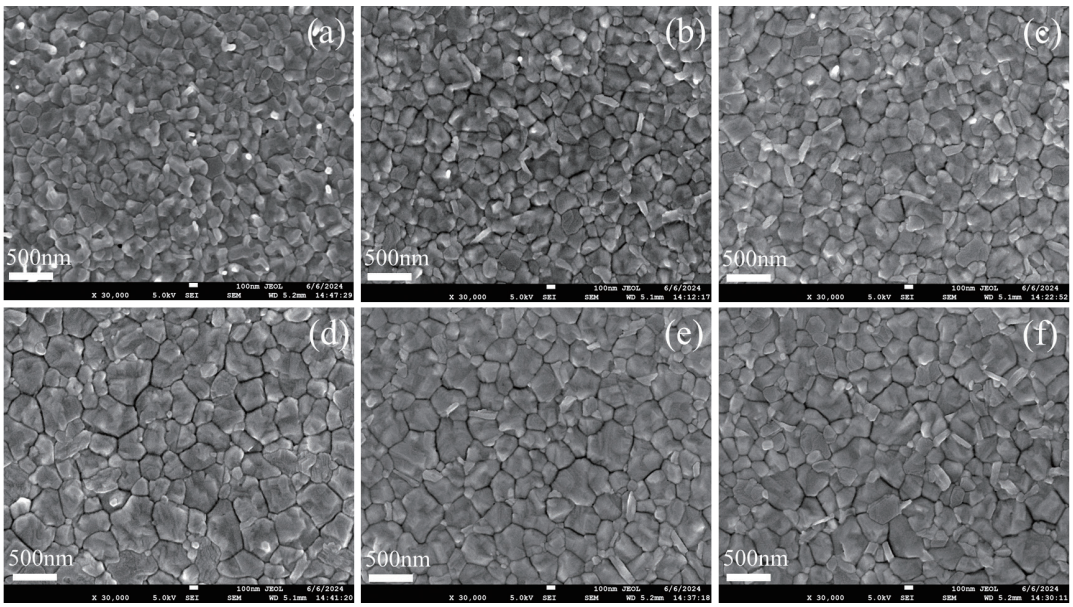

Fig. 1. Top view of perovskite layer. The percentages of CB in the antisolvent are (a) 0%, (b) 10%, (c) 20%, (d) 30%, (e) 40%, and (f) 50%.

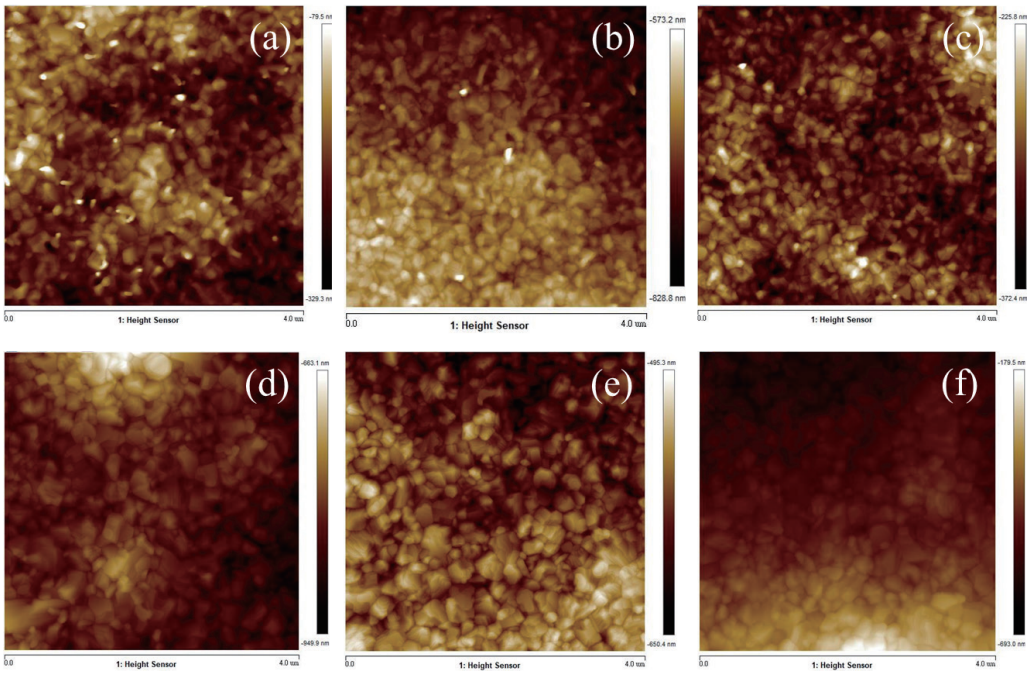

Fig. 2. (Color online) AFM images of perovskite layer. The percentages of CB in the antisolvent are (a) 0%, (b) 10%, (c) 20%, (d) 30%, (e) 40%, and (f) 50%.

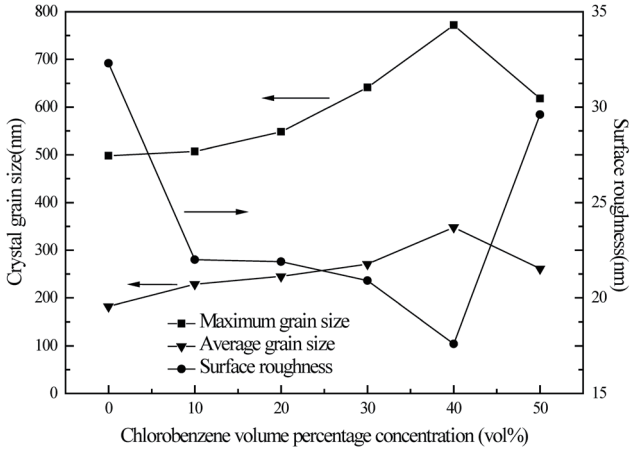

Fig. 3. Maximum grain size (solid squares), average grain size (solid inverted triangles), and surface roughness (solid circles).

increased from 182 to 348 nm and from 498 to 772 nm at the CB ratios of 0 and 40 vol%, respectively. At a CB ratio of 50 vol%, the average grain size decreased to 261 nm, whereas the maximum grain size was 618 nm. In the absence of CB, the surface roughness of the perovskite was 34 nm. As the CB ratio increased, the surface roughness decreased. At a ratio of 40 vol%, the lowest surface roughness was 17.6 nm. At a ratio of 50 vol%, the surface roughness reached 29.6 nm.

Figure 4 shows the UV–Vis spectra of a perovskite film. With MA and CB, the absorption gradually increased. With MA mixed with 40 vol% CB, the absorption of the perovskite layer became the highest. With MA mixed with 50 vol% CB, the absorption decreased. The higher the absorption, the better the photoelectric conversion efficiency.

Figure 5 shows the XRD patterns of the perovskite layer with the antisolvents. With MA only, the diffraction peak of the perovskite film became low. At 14.2°, the strongest peak represented the main crystal face (110) of the perovskite layer. At 28.5° and 31.9°, significant secondary peaks of (220) and (310) were observed, respectively.[18] With MA mixed with 40 vol% CB, the diffraction peaks were the highest. The stronger the diffraction peak, the better the crystallinity and the larger the grain size of the perovskite film.

In this study, we used MA mixed with CB to improve the maximum grain size, minimum surface roughness, and best PCE at 40 vol% CB, as shown in Fig. 6. Cao *et al.* compared the particle size and PCE of single antisolvent and mixed antisolvents prepared by mixing CB with perylene.[19] The largest particle size and a PCE of 20.05% were obtained when CB was mixed with 4 μg/ml perylene.[19]

Although our PCE did not exceed 20% in the entire experiment, we could see that our 40 vol% CB had the best performance when the perovskite layer processing conditions were different. Therefore, we believe this effect was achieved by using the mixed antisolvents. To further improve efficiency, research into the electron and hole transport layers would be beneficial. We believe that this method can be useful for other teams working on the one-step perovskite process as a reference for using antisolvents.

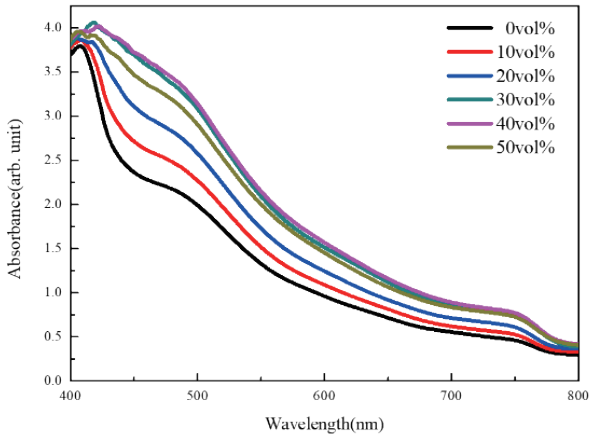

Fig. 4. (Color online) UV–Vis spectra of perovskite prepared using MA mixed with different ratios of CB.

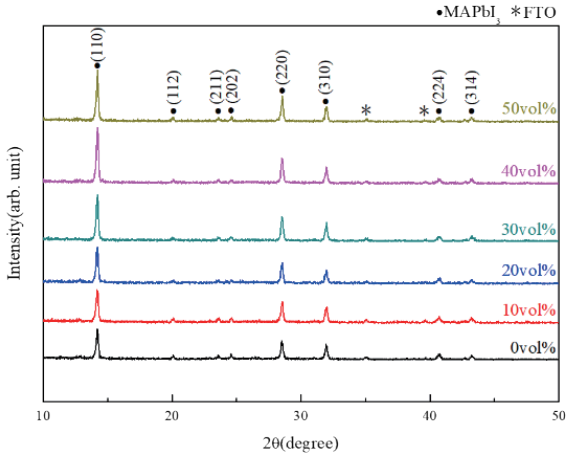

Fig. 5. (Color online) XRD patterns of perovskite prepared using MA mixed with CB.

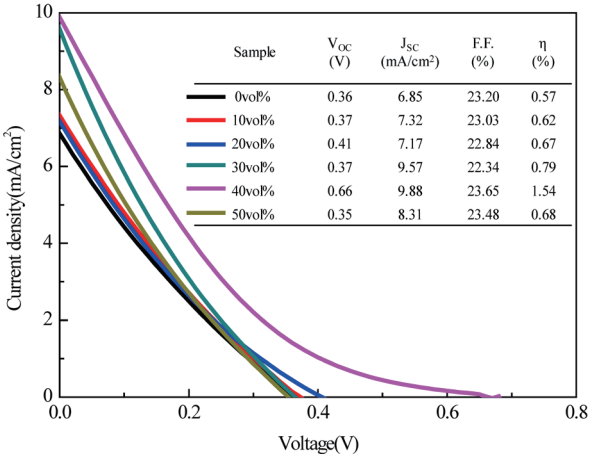

Fig. 6. (Color online) *J–V* curves of perovskite prepared using MA mixed with CB as antisolvent.

In summary, improving surface flatness and particle size is crucial to improving PCE. Using mixed antisolvents can indeed improve the thin film of PSCs and increase the photoelectric conversion efficiency more effectively than using a single antisolvent.[20]

4. Conclusions

In this study, MA was mixed with CB at various ratios as antisolvents to determine the optimal performance of PSCs. The average and maximum grain sizes of the perovskite crystals were 348 and 772 nm, respectively. The lowest surface roughness of 17.6 nm was achieved. Compared with the perovskite crystals formed using pure MA or CB as the antisolvent, an appropriate proportion of CB promotes the formation of perovskite crystals with larger average grain size and more uniform size distribution, which is reflected in the increase in average grain size and the maximum grain size, as well as the decrease in surface roughness. At 40 vol% CB, the optimal optical absorption was achieved, resulting in the highest power conversion efficiency. The open-circuit voltage increased from 0.36 to 0.66 V, the short-circuit current density increased from 6.85 to 9.88 mA/cm^2, the fill factor increased from 23.20 to 23.65%, and the total efficiency improved from 0.57 to 1.54%.

We found that using 40 vol% CB in the mixed antisolvents produced the best overall performance, demonstrating the key role of mixed antisolvents in optimizing the process. To further improve the efficiency of PSCs, future research can focus on optimizing the electron and hole transport layers. We believe that this antisolvent treatment strategy can be a valuable reference for research teams using a one-step method to prepare perovskite films.

Acknowledgments

The authors are grateful to Yu-Jie Liao, Wen-liang Wang, and Pei-Rong Wu for their assistance.

References

1 T. C. Wu, W. M. Huang, J. K. Tsai, C. E. Chang, and T. H. Meen: Coatings **14** (2024) 304. https://doi.org/10.3390/coatings14030304
2 T. H. Meen, J. K. Tsai, Y. S. Tu, T. C. Wu, W. D. Hsu, and S. J. Chang: Nanoscale Res. Lett. **9** (2014) 1. https://doi.org/10.1186/1556-276X-9-523
3 H. J. Snaith: J. Phys. Chem. Lett. **4** (2013) 3623. https://doi.org/10.1021/jz4020162
4 H. Xie, X. Yin, Y. Guo, J. Liu, W. Que, and G. Wang: Phys. Status. Solidi-R. **13** (2019) 1800566. https://doi.org/10.1002/pssr.201800566
5 J. Chen, X. Fan, J. Li, J. Wang, J. Zeng, W. Zhu, and W. Song: J. Mater. Chem. A **12** (2024) 23801. https://doi.org/10.1039/D4TA03926B
6 J. Zhang, C. Shi, J. Chen, Y. Wang, and M. Li: J. Solid State Chem. **238** (2016) 223. https://doi.org/10.1016/j.jssc.2016.03.033
7 T. Leijtens, B. Lauber, G. E. Eperon, S. D. Stranks, and H. J. Snaith: J. Phys. Chem. Lett. **5** (2014) 1096. https://doi.org/10.1021/jz500209g
8 I. Sta, M. Jlassi, M. Hajji, M. F. Boujmil, R. Jerbi, M. Kandyla, M. Kompitsas, and H. Ezzaouia: J. Sol-Gel Sci. Technol. **72** (2014) 421. https://doi.org/10.1007/s10971-014-3452-z
9 N. Kwon, J. Lee, M. J. Ko, Y. Y. Kim, and J. Seo: Nano Convergence **10** (2023) 28. https://doi.org/10.1186/s40580-023-00375-5

10 F. Yang, G. Kapil, P. Zhang, Z. Hu, M. A. Kamarudin, T. Ma, and S. Hayase: ACS Appl. Mater. Interfaces **10** (2018) 16482. https://doi.org/10.1021/acsami.8b02554
11 Q. Tai, P. You, H. Sang, Z. Liu, C. Hu, H. L. Chan, and F. Yan: Nat. Commun. **7** (2016) 11105. https://doi.org/10.1038/ncomms11105
12 X. Liu, C. Xu, and E. C. Lee:ACS. Appl. Energy Mater. **3** (2020) 12291. https://doi.org/10.1021/acsaem.0c02342
13 H. Li, Y. Xia, C. Wang, G. Wang, Y. Chen, L. Guo, D. Luo, and S. Wen: ACS Appl. Mater. Interfaces **11** (2019) 34989. https://doi.org/10.1021/acsami.9b12323
14 A. M. El-Naggar, M. M. Osman, Z. K. Heiba, M. B. Mohamed, A. M. Kamal, A. M. Aldhafiri, and E. A. Alghamdi: J. Mater. Res. Technol. **14** (2021) 287. https://doi.org/10.1016/j.jmrt.2021.06.035
15 Y. Gou, S. Tang, C. Yun, P. Zhao, J. Chen, and H. Yu: Mater. Horiz. **11** (2024) 3465. https://doi.org/10.1039/D4MH00290C
16 S. Raeisi, M. Mohammadi, A. Hoseini, M. Dashti, and Z. Heidary: J. Electron. Mater. **52** (2023) 1419. https://doi.org/10.1007/s11664-022-10120-z
17 M. C. Eze, H. U. Eze, G. N. Ugwuanyi, M. Alnajideen, A. Atia, S. C. Olisa, V. G. Rocha, and G. Min: Organic Electronics **107** (2022) 106552. https://doi.org/10.1016/j.orgel.2022.106552
18 M. I. Hossain, Y. Tong, A. Shetty, and S. Mansour: Sol. Energy **265** (2023) 112128. https://doi.org/10.1016/j.solener.2023.112128
19 Y. Cao, Z. Liu, W. Li, Z. Zhao, Z. Xiao, B. Lei, N. Cheng, J. Liu, and Y. Tu: Sol. Energy **220** (2021) 251. https://doi.org/10.1016/j.solener.2021.03.055
20 S. Yang, Y. Chen, Y. C. Zheng, X. Chen, Y. Hou, and H. G. Yang: RSC Adv. **5** (2015) 69502. https://doi.org/10.1039/C5RA12348H